Applied Physics Letters

High electrical conducting deep-ultraviolet-transparent oxide semiconductor La-doped $SrSnO_3$ exceeding ~3000 S cm^{-1}

Cite as: Appl. Phys. Lett. **116**, 022103 (2020); https://doi.org/10.1063/1.5128410
Submitted: 20 September 2019 . Accepted: 29 December 2019 . Published Online: 13 January 2020

Mian Wei, Anup V. Sanchela, Bin Feng, Yuichi Ikuhara, Hai Jun Cho, and Hiromichi Ohta

Applied Physics Letters ARTICLE scitation.org/journal/apl

High electrical conducting deep-ultraviolet-transparent oxide semiconductor La-doped $SrSnO_3$ exceeding ~3000 S cm^{-1}

Cite as: Appl. Phys. Lett. **116**, 022103 (2020); doi: 10.1063/1.5128410
Submitted: 20 September 2019 · Accepted: 29 December 2019 ·
Published Online: 13 January 2020

Mian Wei,[1] Anup V. Sanchela,[2] Bin Feng,[3] Yuichi Ikuhara,[3] Hai Jun Cho,[1,2,a)] and Hiromichi Ohta[1,2,a)]

AFFILIATIONS

[1]Graduate School of Information Science and Technology, Hokkaido University, N14W9, Kita, Sapporo 060-0814, Japan
[2]Research Institute for Electronic Science, Hokkaido University, N20W10, Kita, Sapporo 001-0020, Japan
[3]Institute of Engineering Innovation, The University of Tokyo, 2 – 11–16 Yayoi, Bunkyo, Tokyo 113-8656, Japan

[a)]**Authors to whom correspondence should be addressed:** joon@es.hokudai.ac.jp and hiromichi.ohta@es.hokudai.ac.jp

ABSTRACT

La-doped $SrSnO_3$ (LSSO) is known as one of the deep-ultraviolet (DUV)-transparent conducting oxides with an energy bandgap of ~4.6 eV. Since LSSO can be grown heteroepitaxially on more wide bandgap substrates such as MgO (E_g ~ 7.8 eV), LSSO is considered to be a good candidate for a DUV-transparent electrode. However, the electrical conductivity of LSSO films is below 1000 S cm^{-1}, most likely due to the low solubility of the La ion in the LSSO lattice. Here, we report that high electrically conducting (>3000 S cm^{-1}) LSSO thin films with an energy bandgap of ~4.6 eV can be fabricated by pulsed laser deposition on a MgO substrate followed by a simple annealing in vacuum. From the X-ray diffraction and the scanning transmission electron microscopy analyses, we found that lateral grain growth occurred during the annealing, which improved the activation rate of the La ion, leading to a significant improvement of the carrier concentration (3.26×10^{20} cm^{-3}) and Hall mobility (55.8 cm^2 V^{-1} s^{-1}). The present DUV-transparent oxide semiconductor would be useful as a transparent electrode for developing optoelectronic devices, which transmit and/or emit DUV-light.

Deep-ultraviolet (DUV, 200–300 nm in wavelength) transparent oxide semiconductors[1] have attracted attention as transparent electrodes for DUV optoelectronic devices such as DUV light emitting diodes and DUV detectors for biological applications because most DNAs show their absorption peaking around 260 nm in wavelength.[2] Although conventional transparent oxide semiconductors such as Al-doped ZnO and Sn-doped In_2O_3 (ITO) are opaque in the DUV region (wavelength $\lambda < 300$ nm) due to their small bandgaps (E_g ~3.2 eV), DUV transparent oxide semiconductors are transparent in the DUV region. Among several DUV transparent oxide semiconductors, La-doped $SrSnO_3$ (E_g ~4.6 eV,[3–6] LSSO hereafter) would be the most promising material because LSSO can be grown heteroepitaxially on single crystalline substrates such as MgO,[7] $SrTiO_3$,[8] and $KTaO_3$.[9] Further, the electrical conductivity of LSSO films (~1000 S cm^{-1})[10] is larger than that of well-known DUV transparent oxide semiconductors such as β-Ga_2O_3 (E_g ~ 4.9 eV, ~1 S cm^{-1}),[11,12] α-Ga_2O_3 (E_g ~ 5.3 eV, ~0.3 S cm^{-1}),[13] electron-doped calcium aluminate (C12A7:e^-, ~4 eV, ~800 S cm^{-1}),[14–16] and recently developed Al:$Mg_{0.43}Zn_{0.57}O$ (E_g ~ 4.2 eV, ~400 S cm^{-1}).[17] However, the electrical conductivity of LSSO films is still lower than that of commercially available transparent conducting oxide ITO (~7000 S cm^{-1}).

The crystal structure of $SrSnO_3$ is regarded as a pseudo-double-cubic perovskite ($a = 0.8068$ nm)[18] though the real lattice is orthorhombic.[19] Several researchers fabricated the epitaxial films of LSSO by using the vapor phase epitaxy method such as pulsed laser deposition (PLD)[8–10] and molecular beam epitaxy (MBE).[20] However, due to difficulties in growing high-quality LSSO films, their electron transport properties have not been extensively studied compared to the optical properties and electronic structures. Baba *et al.*[10] reported that the electrical conductivity of the 5% La-doped LSSO film on the lattice matched $NdScO_3$ substrate by PLD was ~1000 S cm^{-1}, which is the highest electrical conductivity ever reported. However, the carrier concentration was only 2.5×10^{20} cm^{-3}, which is ~1/3 of the La concentration [La], indicating a low activation rate of La. We hypothesized that the electrical conductivity of LSSO films can be improved if the solubility of La ions in the LSSO lattice is enhanced.

In order to enhance the solubility of La ions in the LSSO films, we simply annealed the LSSO films at 790 °C in vacuum (<10^{-2} Pa).

Generally, sintering of n-type oxide semiconductors becomes faster when the point defect (oxygen vacancy) is formed. For example, Al-doped ZnO is generally sintered under a reducing atmosphere. We expected that the point defect formation during the annealing in vacuum would induce grain growth and increase the solubility of the La ion. After annealing, we indeed observed grain growth of PLD-grown LSSO films from ~10 nm to ~28 nm, and the electron transport properties of the annealed LSSO films were significantly improved. Here, we report that high electrically conducting (>3000 S cm^{-1}) LSSO thin films were fabricated by pulsed laser deposition on the MgO [E_g ~ 7.8 eV (Ref. 21)] substrate followed by the simple annealing in vacuum. The significant improvement of the carrier concentration (3.26 × 10^{20} cm^{-3}) and Hall mobility (55.8 cm^2 V^{-1} s^{-1}) occurred after the annealing. The present DUV-transparent oxide semiconductor would be useful as the transparent electrode to develop optoelectronic devices, which transmit and/or emit DUV-light.

$La_xSr_{1-x}SnO_3$ (x = 0.005, 0.02, 0.03, and 0.05) epitaxial films were fabricated on (001) MgO (a = 0.4212 nm) single crystal substrates using the PLD technique (KrF excimer laser, λ = 248 nm, fluence ~2 J cm^{-2} $pulse^{-1}$, and repetition rate = 10 Hz). During the film growth, the substrate temperature and oxygen pressure inside the chamber were kept at 790 °C and 20 Pa, respectively. Note that the conducting LSSO film was not obtained when the oxygen pressure was lower than 20 Pa, indicating that oxygen vacancies do not act as the electron donor, similar to La-doped $BaSnO_3$.[22] After the film growth, we turned off the substrate heater immediately and cooled the sample down to room temperature. The crystalline phase, orientation, lattice parameters, and thickness of the films were analyzed by high resolution X-ray diffraction (Cu $K\alpha_1$, ATX-G, Rigaku Co.). The out-of-plane Bragg diffraction patterns and the rocking curves were recorded at room temperature. X-ray reflection patterns were recorded to evaluate the density and the thickness. Atomic force microscopy (AFM, Nanocute, Hitachi Hi-Tech Sci. Co.) was used to observe the surface microstructure of the films.

In order to clarify the change of the lateral grain size, we measured the X-ray reciprocal space mapping (RSM) of the resultant LSSO film (x = 0.03, as-grown) around the 204 diffraction spot of LSSO [Fig. 1(a)]. A broad diffraction spot of 204 LSSO is seen peaking

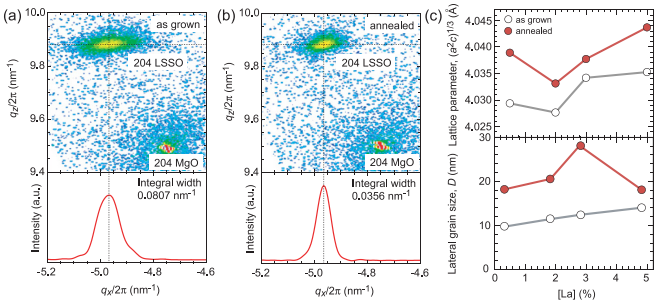

FIG. 1. Lateral grain growth of the LSSO films by vacuum annealing. (a) and (b) RSMs around the 204 LSSO diffraction spot of the (a) as-grown and (b) annealed films. The cross-sectional diffraction patterns along the $q_x/2\pi$ direction are shown at the bottom of each RSM. (c) Changes in (upper) the average lattice parameter and (lower) lateral grain size of the as-deposited LSSO films (white) and annealed LSSO films (red) as a function of La concentration in the target materials. The vacuum annealing substantially increased the lateral grain size.

at ($q_x/2\pi$, $q_z/2\pi$) = (−4.97 nm^{-1}, 9.88 nm^{-1}) together with the 204 diffraction spot of MgO at (−4.75 nm^{-1}, 9.50 nm^{-1}), indicating that incoherent epitaxial growth occurred. The lateral grain size was ~12 nm, which was calculated by Scherrer's equation, D = (integral width)$^{-1}$, using the cross-sectional diffraction pattern along the $q_x/2\pi$ direction.

In order to increase the lateral grain size, we annealed the LSSO films at 790 °C in vacuum (<10^{-2} Pa) for 30 min and cooled down to room temperature. After the vacuum annealing, the 204 diffraction spot intensity increased as shown in Fig. 1(b), and the lateral grain size was successfully increased up to 28 nm. A similar increase in the diffraction spot intensity was observed in all cases (x = 0.005, 0.02, and 0.05) as shown in supplementary material Figs. S1(a)−S1(h). Using the 204 diffraction spots, we determined the average lattice parameters $(a^2 \times c)^{1/3}$ of the LSSO films before and after annealing [Fig. 1(c)]. The annealed films showed more relaxation, which is likely attributed to the grain growth and the improvements in the solubility of the La ion. Note that we optimized the annealing condition by annealing under several atmospheres including air, 1 Pa oxygen, and vacuum (<10^{-2} Pa) (data not shown). Significant grain growth was observed when the LSSO film was annealed in vacuum. This is consistent with the fact that the accelerated dislocation movement occurs due to oxygen vacancy-assisted recovery in ionic crystals.[23] Therefore, we fixed the annealing atmosphere as vacuum. According to previous studies on stannate films, extra charge carriers from oxygen vacancies are compensated by the formation of charge accepting A-site vacancies.[24,25] Therefore, any carrier concentration changes that may result from the vacuum annealing are likely attributed to the activation of La dopants. In addition, we did not obtain any conducting film when we annealed the undoped $SrSnO_3$ film in vacuum. It means that the oxygen vacancy does not significantly affect carrier generation.

In order to further confirm the grain growth due to the vacuum annealing, the microstructures of the LSSO films were observed using low-angle annular dark-field scanning transmission electron microscopy (LAADF-STEM). While columnar structures were observed for both the as-deposited [Fig. 2(a)] and annealed LSSO films [Fig. 2(b)], the width of the columns for the annealed LSSO film was significantly greater. This indicates that the vacuum annealing indeed induces grain growth, which is in excellent agreement with the RSM results. It should be noted that incoherent interfaces with misfit dislocations were observed at the interface between the LSSO film and the MgO substrate in both cases as shown in supplementary material Figs. S2(a) and S2(b), indicating that the interface structures are not affected by the vacuum annealing.

Then, the electrical conductivity (σ), carrier concentration (n), and Hall mobility (μ_{Hall}) of the films were measured using the conventional dc four-probe method with van der Pauw electrode geometry at room temperature. The thermopower (S) was acquired from the thermoelectromotive force (ΔV) generated by a temperature difference (ΔT) of ~4 K across the film using two Peltier devices. The temperatures at each end of the films were simultaneously measured with two thermocouples, and the S-values were calculated from the slope of the ΔT–ΔV plots (correlation coefficient: >0.9999).

Figure 3 summarizes the electron transport properties of the resultant LSSO films at room temperature. Both the carrier concentration and Hall mobility gradually increased with [La] until [La] = 3% and decreased at [La] = 5%, probably due to the low solubility limit of

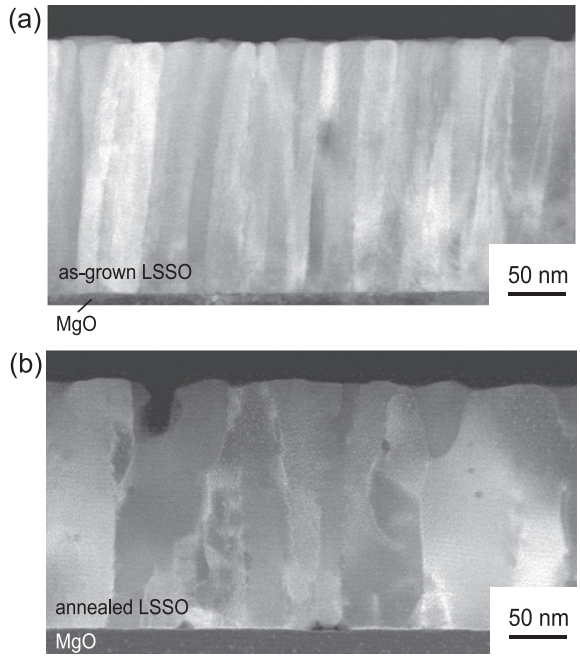

FIG. 2. Cross-sectional LAADF-STEM images of the LSSO films [(a) as-grown and (b) annealed LSSO films]. The lateral grain growth of the annealed LSSO films is clearly visualized.

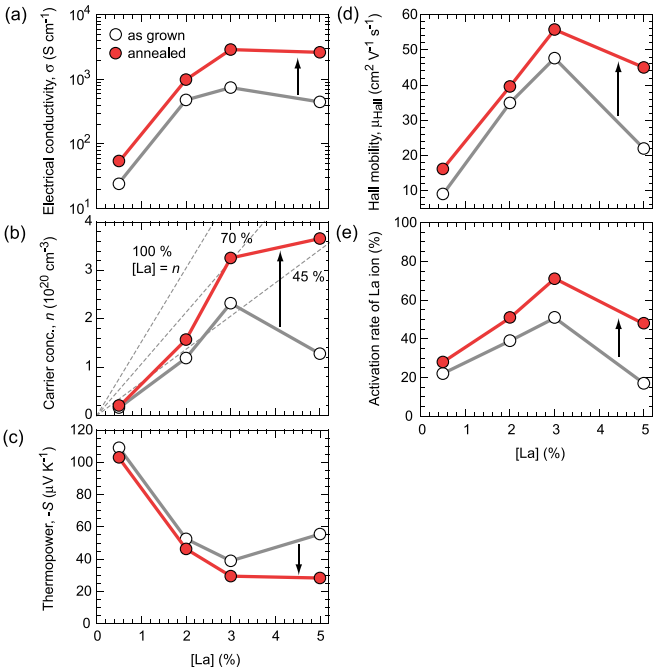

FIG. 3. Electron transport properties of the resultant LSSO thin films as a function of La component (%) in the target materials at room temperature. (a) Electrical conductivity (σ); enhancement of σ for the vacuum annealed LSSO films increased with the La component. (b) Carrier concentration (n); n of the LSSO film increased after annealing in vacuum. (c) Thermopower ($-S$); the absolute value of thermopower (S) decreased after annealing. (d) Hall mobility (μ_{Hall}); the μ_{Hall} of the annealed LSSO films was largely enhanced at 5% La^{3+}. (e) Activation rate of the La ion; after vacuum annealing, the La ion became more active.

La in the $SrSnO_3$ lattice. This is similar to $BaSnO_3$.[26] Significant enhancements in the electron transport properties were observed in the vacuum annealed LSSO films. Compared to the as-grown LSSO films, the annealed LSSO films showed greater σ [Fig. 3(a)], n [Fig. 3(b)], and μ_{Hall} [Fig. 3(d)] at room temperature. The largest enhancement was observed in the 5% La doped LSSO film. The absolute value of S for LSSO films decreased after annealing [Fig. 3(c)]. This is consistent with the fact that the carrier concentration increased after annealing. The activation rate of the La ion [Fig. 3(e)], which was calculated as $n\cdot[La]^{-1}$, assuming that the La^{3+} ion solely generated carrier electrons, increased after the vacuum annealing. Thus, the increased σ and μ_{Hall} of annealed films are probably attributed to the improved efficiency of the carrier activation from the La dopant and the grain growth. Therefore, carrier electrons are more efficiently provided in the annealed films. The highest σ and μ_{Hall} were observed at annealed 3%-La doped LSSO films, whose activation of the La ion and lateral grain size showed the largest value.

In this study, the experimental electron effective mass (m^*) value of the LSSO epitaxial films was also clarified by the relationship of thermopower (S) and carrier concentration (n) of the resultant films at room temperature [Fig. 4(a)]. Since both n and S values are only sensitive to the density of states and Fermi level, we calculated m^* using the following equations:[27]

$$S = -\frac{k_B}{e}\left(\frac{(r+2)F_{r+1}(\xi)}{(r+1)F_r(\xi)} - \xi\right), \tag{1}$$

where k_B, ξ, r, and F_r are the Boltzmann constant, reduced Fermi energy, scattering parameter of relaxation time, and Fermi integral, respectively. We assumed the r value of 0.5 (optical phonon scattering) because the temperature dependence of Hall mobility showed that phonon scattering is dominant at room temperature (data not shown). F_r and n are given by

$$F_r(\xi) = \int_0^\infty \frac{x^r}{1+e^{x-\xi}}dx, \tag{2}$$

$$n_- = 4\pi\left(\frac{2m^*k_BT}{h^2}\right)^{3/2} F_{1/2}(\xi), \tag{3}$$

where h and T are the Planck constant and absolute temperature, respectively. Most of the S–n plots ($n > 10^{20}\,cm^{-3}$) are located on the line obtained m^* of 0.23 m_0, similar to that of $Ba_{0.5}Sr_{0.5}SnO_3$,[28] though two plots ($n < 10^{20}\,cm^{-3}$) are located on the lower side, probably due to the contribution of the tail state around the conduction band minimum.

Figure 4(b) summarizes the Hall mobility (μ_{Hall}) of the LSSO epitaxial films as a function of carrier concentration (n) at room temperature. The values reported by Wang *et al.*[20] and Baba *et al.*[10] are also plotted for comparison. The μ_{Hall} increased with increasing n. The highest μ_{Hall} and electrical conductivity were observed from the 3% La-doped LSSO film. The μ_{Hall} reached 55.8 $cm^2\,V^{-1}\,s^{-1}$ at a carrier concentration of $3.26\times10^{20}\,cm^{-3}$, which is highest value ever reported in the LSSO film to date. Moreover, we achieved an electrical conductivity exceeding 3000 S cm^{-1} in the annealed 3% La-doped

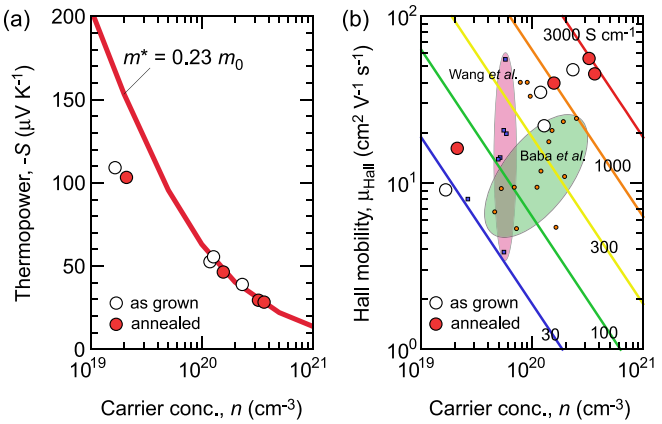

FIG. 4. (a) Thermopower ($-S$) and (b) Hall mobility (μ_{Hall}) of the resultant LSSO films as a function of carrier concentration (n) at room temperature. The carrier effective mass (m^*) value of LSSO is 0.23 m_0, clarified by the thermopower measurements. By the thermal annealing in vacuum, we achieved the electrical conductivity exceeding 3000 S cm^{-1} in the LSSO film and the mobility reaches a value as high as 55.8 cm^2 V^{-1} s^{-1} at a carrier concentration of 3.26 × 10^{20} cm^{-3}. The values reported by Wang *et al.*[20] (blue square) and Baba *et al.*[10] (orange circle) are also plotted for comparison.

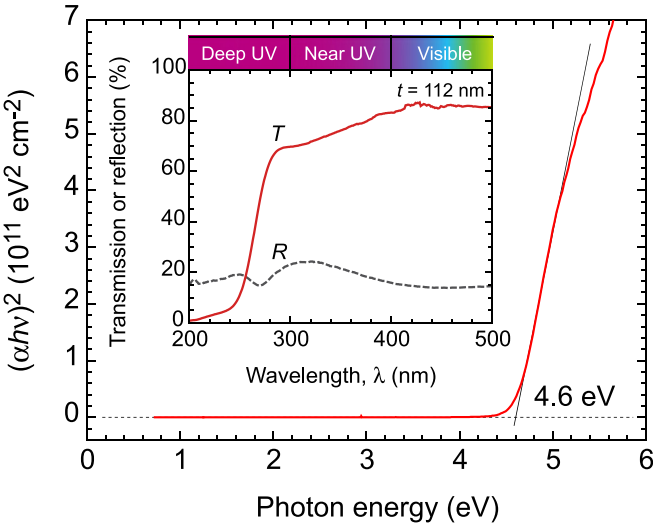

FIG. 5. Optical bandgap of the resultant 3% La-doped LSSO thin film. The E_g was ~4.6 eV, which was obtained from the linear relationship of $(\alpha h\nu)^2$–photon energy with assuming the direct bandgap. The absorption coefficient α was obtained from the transmission and reflection data shown in the inset.

LSSO film, which is much higher than that of other DUV transparent conducting oxides such as electron doped β-Ga_2O_3 (E_g ~4.9 eV, ~1 S cm^{-1}),[11,12] α-Ga_2O_3 (E_g ~5.3 eV, ~0.3 S cm^{-1}),[13] C12A7:e^-, ~4 eV, ~800 S cm^{-1})[1,4–16] and recently developed Al:$Mg_{0.43}Zn_{0.57}O$ (E_g ~ 4.2 eV, ~400 S cm^{-1}).[17]

Finally, we measured the optical transmission and reflection spectra of the 3% La-doped LSSO film (thickness: 112 nm) grown on the double side polished (001) MgO substrate followed by the vacuum annealing at 790 °C (inset of Fig. 5). The optical transmission in the deep UV region was kept ~70% at 300 nm in wavelength and exceeded 25% at 260 nm in wavelength, which is the absorption peak wavelength of most DNAs.[2] Although $SrSnO_3$ has an indirect bandgap,[29] we estimated the bandgap by assuming a direct bandgap; the $(\alpha \times h \times \nu)^2$–photon energy plot was used to estimate the bandgap of the LSSO film (Fig. 5), where α is the absorption coefficient and ν is the speed of light. The bandgap was ~4.6 eV, agreeing well with the reported values.[3–5] The α at 260 nm in wavelength was calculated to be 8.3×10^4 cm^{-1}; the penetration depth of 260 nm light is ~120 nm, which is the origin of low transmission (25%) of the 260 nm light through the LSSO film (112 nm). Thus, most of the 260 nm light can transmit through the LSSO film when the thickness is thinner. From these results, we concluded that the present LSSO film, which exhibited a high electrical conductivity of ~3000 S cm^{-1} and deep UV transparency, would be useful as the transparent electrode to develop optoelectronic devices, which transmit and/or emit DUV-light, especially for biological applications. The figure-of-merit φ_{TC}[30] ($=T^{10}/R_s$, T is the transmission and R_s is the sheet resistance) of the present LSSO film is 14.5×10^{-3} Ω^{-1}, which is four orders magnitude larger than that of β-Ga_2O_3 ($\varphi_{TC} = 7.8 \times 10^{-7}$ Ω^{-1}), at 300 nm in wavelength.

In summary, we fabricated high electrically conducting (>3000 S cm^{-1}) LSSO thin films with an energy bandgap of ~4.6 eV by a pulsed laser deposition on a MgO substrate followed by the simple annealing in vacuum. From the X-ray diffraction and the scanning transmission microscopy analyses, we found that lateral grain growth occurred during the annealing, which improves the activation rate of the La ion, leading to the significant improvement of carrier concentration (3.26×10^{20} cm^{-3}) and Hall mobility (55.8 cm^2 V^{-1} s^{-1}). The bandgap was ~4.6 eV. The optical transmission at 300 nm in wavelength was ~70% and that at 260 nm in wavelength exceeded 25%. The present DUV-transparent oxide semiconductor would be useful as the transparent electrode to develop optoelectronic devices, which transmit and/or emit DUV-light, especially for biological applications.

See the supplementary material for the RSM near the 204 diffraction spot of the LSSO films and the cross-sectional high-angle annular dark-field scanning transmission electron microscopy (HAADF-STEM) images for the LSSO films.

This research was supported by Grants-in-Aid for Scientific Research A (No. 17H01314) and Innovative Areas (Nos. 19H05791 and 19H05788) from the JSPS. A part of this work was supported by Dynamic Alliance for Open Innovation Bridging Human, Environment, and Materials and by the Network Joint Research Center for Materials and Devices. H.J.C. acknowledges the support from the Nippon Sheet Glass Foundation for Materials Science and Engineering. H.O. acknowledges the support from the Asahi Glass Foundation and the Mitsubishi Foundation. The support from the China Scholarship Council (M. Wei, No. 201808050081) is also greatly appreciated.

The authors declare no competing financial interest.

REFERENCES

[1]D. Ginley, H. Hosono, and D. C. Paine, *Handbook of Transparent Conductors* (Springer, 2011).
[2]L. M. Xiang, J. L. Palma, Y. Q. Li, V. Mujica, M. A. Ratner, and N. J. Tao, Nat. Commun. **8**, 14471 (2017).

[3]H. Mizoguchi, H. W. Eng, and P. M. Woodward, Inorg. Chem. **43**, 1667 (2004).
[4]D. J. Singh, Q. Xu, and K. P. Ong, Appl. Phys. Lett. **104**, 011910 (2014).
[5]Q. Z. Liu, F. Jin, G. Y. Gao, and W. Wang, J. Alloys Compd. **717**, 62 (2017).
[6]Q. Gao, H. L. Chen, K. F. Li, and Q. Z. Liu, ACS Appl. Mater. Interfaces **10**, 27503 (2018).
[7]Y. Yamamoto, M. Mukaida, A. Ichinose, K. Matsumoto, Y. Yoshida, S. Horii, A. Saito, and S. Ohshima, Physica C **412**, 1316 (2004).
[8]M. C. F. Alves, S. Boursicot, S. Ollivier, V. Bouquet, S. Deputier, A. Perrin, I. T. Weber, A. G. Souza, I. M. G. Santos, and M. Guilloux-Viry, Thin Solid Films **519**, 614 (2010).
[9]H. M. Christen, L. A. Boatner, J. D. Budai, M. F. Chisholm, C. Gerber, and M. Urbanik, Appl. Phys. Lett. **70**, 2147 (1997).
[10]E. Baba, D. Kan, Y. Yamada, M. Haruta, H. Kurata, Y. Kanemitsu, and Y. Shimakawa, J. Phys. D **48**, 455106 (2015).
[11]M. Orita, H. Ohta, M. Hirano, and H. Hosono, Appl. Phys. Lett. **77**, 4166 (2000).
[12]R. Wakabayashi, K. Yoshimatsu, M. Hattori, and A. Ohtomo, Appl. Phys. Lett. **111**, 162101 (2017).
[13]T. Kawaharamura, G. T. Dang, and M. Furuta, Jpn. J. Appl. Phys., Part 1 **51**, 040207 (2012).
[14]K. Hayashi, S. Matsuishi, T. Kamiya, M. Hirano, and H. Hosono, Nature **419**, 462 (2002).
[15]S. Matsuishi, Y. Toda, M. Miyakawa, K. Hayashi, T. Kamiya, M. Hirano, I. Tanaka, and H. Hosono, Science **301**, 626 (2003).
[16]M. Miyakawa, M. Hirano, T. Kamiya, and H. Hosono, Appl. Phys. Lett. **90**, 182105 (2007).
[17]D. Zhang, W. Zheng, Q. H. Zheng, A. Q. Chen, X. Ji, and F. Huang, Adv. Electron. Mater. **2**, 1600320 (2016).
[18]A. J. Smith and A. J. E. Welch, Acta Crystallogr. **13**, 653 (1960).
[19]A. Vegas, M. Valletregi, J. M. Gonzalezcalbet, and M. A. Alariofranco, Acta Crystallogr., Sect. B **42**, 167 (1986).
[20]T. Q. Wang, L. R. Thoutam, A. Prakash, W. Nunn, G. Haugstad, and B. Jalan, Phys. Rev. Mater. **1**, 061601(R) (2017).
[21]O. E. Taurian, M. Springborg, and N. E. Christensen, Solid State Commun. **55**, 351 (1985).
[22]A. Sanchela, M. Wei, J. Lee, G. Kim, H. Jeen, B. Feng, Y. Ikuhara, H. J. Cho, and H. Ohta, J. Mater. Chem. C **7**, 5797 (2019).
[23]D. Yoon, S. Yu, and J. Son, NPG Asia Mater. **10**, 363 (2018).
[24]L. Weston, L. Bjaalie, K. Krishnaswamy, and C. G. Van de Walle, Phys. Rev. B **97**, 054112 (2018).
[25]H. J. Cho, B. Feng, T. Onozato, M. Wei, A. Sanchela, Y. Ikuhara, and H. Ohta, Phys. Rev. Mater. **3**, 094601 (2019).
[26]A. V. Sanchela, T. Onozato, B. Feng, Y. Ikuhara, and H. Ohta, Phys. Rev. Mater. **1**, 034603 (2017).
[27]C. B. Vining, J. Appl. Phys. **69**, 331 (1991).
[28]A. V. Sanchela, M. Wei, H. J. Cho, and H. Ohta, Small **15**, 1805394 (2019).
[29]E. Moreira, J. M. Henriques, D. L. Azevedo, E. W. S. Caetano, V. N. Freire, and E. L. Albuquerque, J. Solid State Chem. **184**, 921 (2011).
[30]G. Haacke, J. Appl. Phys. **47**, 4086 (1976).